Angle-of-arrival anemometry by means of a large-aperture Schmidt–Cassegrain telescope equipped with a CCD camera

Yonghun Cheon,* Vincent Hohreiter, Mario Behn, and Andreas Muschinski

Department of Electrical and Computer Engineering, University of Massachusetts, Amherst, 151 Holdsworth Way, Amherst, Massachusetts 01003-9284, USA
**Corresponding author: cheon@mirsl.ecs.umass.edu*

Received March 21, 2007; revised July 10, 2007; accepted August 10, 2007;
posted August 30, 2007 (Doc. ID 81236); published October 12, 2007

The frequency spectrum of angle-of-arrival (AOA) fluctuations of optical waves propagating through atmospheric turbulence carries information of wind speed transverse to the propagation path. We present the retrievals of the transverse wind speed, v_b, from the AOA spectra measured with a Schmidt–Cassegrain telescope equipped with a CCD camera by estimating the "knee frequency," the intersection of two power laws of the AOA spectrum. The rms difference between 30 s estimates of v_b retrieved from the measured AOA spectra and 30 s averages of the transverse horizontal wind speed measured with an ultrasonic anemometer was 11 cm s^{-1} for a 1 h period, during which the transverse horizontal wind speed varied between 0 and 80 cm s^{-1}. Potential and limitations of angle-of-arrival anemometry are discussed © 2007 Optical Society of America

OCIS codes: 010.1300, 010.1330, 010.7350.

1. INTRODUCTION

When an optical wave propagates through atmospheric turbulence, the wave is affected by the refractive-index fluctuations along the optical path. In particular, the angles-of-arrival (AOAs) of a wave incident upon a receiving aperture, or upon the receiver of a two-point interferometer, are functions of the mean values and fluctuations of the refractive-index gradient along the propagation path. Since temporal changes of the local (optical) refractive-index gradient are dominatingly determined by the local wind field and the local temperature field, the temporal characteristics of the AOA fluctuations observed with a telescope or an interferometer carry information about both the wind field and the temperature field along the propagation path.

Assuming that AOAs are measured with a two-point interferometer with a baseline b, and assuming that Taylor's frozen-turbulence hypothesis {Eq. (7) in [1]} and Rytov's approximation (see pp. 124 ff. in [2]) are valid, Tatarskii {Eqs. (33)–(36) on p. 268 and Eq. (40) on p. 269 in [3]} developed a theoretical model of the frequency spectrum of AOA fluctuations of a plane wave propagating through homogeneous and isotropic turbulence. The frequency spectrum is predicted to be proportional to $f^{-2/3}$ for the low-frequency portion ($f<f_k$) and to $f^{-8/3}$ for the high-frequency portion ($f>f_k$), where f is the frequency and f_k is the "knee-frequency," defined as the intersection point of the two asymptotes. Gurvich *et al.* [4] measured the frequency spectrum of AOA fluctuations of a plane wave by using a receiver with an aperture of 8 cm and a propagation path length of 650 m. They reported a time-averaged transverse wind speed of ~ 2 m s^{-1}. They compared the measured frequency spectrum with Tatarskii's theoretical model and also retrieved a transverse wind speed of 2 m s^{-1}, indicating some initial agreement between theory and experiment. They did not mention in detail, however, the manner in which the transverse wind speed was obtained from the frequency spectrum. Nor did they quantify estimation errors or other errors.

Clifford [5] later investigated the frequency spectrum of AOA fluctuations of a spherical wave observed with a two-point interferometer and obtained results similar to Tatarskii's, but with a different weighting function. Rao *et al.* [6] studied numerically the high-frequency behavior of the frequency spectra of log-amplitude, phase, and AOA fluctuations for spherical waves propagating through locally isotropic turbulence and evaluated the effect of the inner scale of turbulence on the high-frequency portion of the frequency spectra. They showed that for turbulence models that include the inner scale of turbulence, the frequency spectrum drops off steeper than −8/3 at high frequencies, where viscous smoothing becomes important.

Recently, Lüdi and Magun [7] developed a theoretical model and conducted experiments for the frequency spectra of two-dimensional AOAs for a millimeter wave propagating through anisotropic turbulence. They fitted their model to the measured spectra and retrieved outer scales of turbulence for the horizontal and vertical directions. The measured spectrum for the horizontal direction for the low frequencies corresponding to the outer scale of turbulence was smaller than that for the vertical direction. By fitting the theoretical model to the measured spectrum, they found that the outer scale of turbulence for the horizontal direction was larger than that for the vertical direction in the case of a stable and stratified atmosphere.

The overwhelming majority of theoretical and experimental work in the area of optical wave propagation

 © 2007 Optical Society of America

through the turbulent atmosphere has focused on amplitude fluctuations (scintillation). The few studies on AOAs ("quivering" and "image motion") were aimed mostly at verifying theoretical predictions of asymptotic power laws. The usefulness of AOA spectra for the retrieval of wind velocities, however, has not been studied in detail yet.

In this paper, we present AOA anemometry as a method for retrieving the path-averaged transverse wind speed from the frequency spectra of AOA fluctuations. Field measurements were conducted at the Boulder Atmospheric Observatory (BAO) near Erie, Colorado. The optical equipment consisted of a commercial Schmidt–Cassegrain telescope with an aperture diameter of 36 cm, a CCD camera, and krypton flashlight bulbs. An ultrasonic anemometer was used to measure the transverse wind speed independently.

This paper is organized as follows. In Section 2, the theory for the spectrum of AOA fluctuations for the spherical wave is summarized, and the knee frequency is defined. In Section 3, each instrument is described, as well as how the instruments were set up. In Section 4, the calculation of AOAs and the retrieval of the path-averaged transverse wind speed from the frequency spectrum of AOA fluctuations are discussed. In Section 5, the experimental results are presented, and path-averaged transverse wind speeds retrieved from the frequency spectra of AOA fluctuations are compared with the transverse wind speeds measured by the ultrasonic anemometer. A summary and conclusions are given in Section 6.

2. THEORY

Let us assume that an optical wave propagates through homogeneous and isotropic turbulence and is observed by a telescope at a distance L from a light source. Let us define the x axis as the propagation direction from the source to the telescope, and the y and z axes such that a right handed coordinate system is formed with the xy plane parallel to the ground and the z axis pointing upward.

To interpret our measured AOA spectra, one needs a theory that describes the experimental setup with sufficient accuracy. According to Tatarskii [3], Clifford [5], and Lawrence and Strohbehn [8], the essential physics of AOA spectra observed with a filled aperture is captured with a rigorous theory of AOA spectra observed with a two-point interferometer. Lawrence and Strohbehn (p. 1542 in [8]) argue, "…if one is using an interferometer, then the angle of arrival is the phase difference measured at two points separated by some distance, call it b. Obviously, the parameter b affects the measurements. If a telescope is used, the angle of arrival is closely related to the average tilt of the wave across the aperture of the telescope. In this case spatial variations in phase tend to average out if they are smaller than the diameter of the aperture." From this statement, one might expect that high-frequency spectral densities of filled-aperture AOAs are lower than those of interferometric AOAs, which may lead to a steeper dropoff for filled-aperture as opposed to interferometric AOA spectra. However, Clifford (p. 1290 in [5]), without offering a proof, claims that the main result of his interferometric theory "also applies to about the same order of approximation for a telescope of diameter b." It is not clear whether his statement is meant to imply that the power law of telescopic and interferometric AOA spectra should be the same.

In this paper, we use Clifford's heuristic argument as a working hypothesis and interpret our telescopic AOA spectra on the basis of his theory [5] of spherical-wave AOA spectra observed with a two-point interferometer. In Subsection 2.A, we discuss Clifford's theory in some detail and show that his main result can be obtained by neglecting diffraction effects. In Subsection 2.B, we come back to the question of the differences between filled-aperture and interferometric AOA spectra.

A. Reevaluation of Clifford's (1971) Theory of the Interferometric AOA Frequency Spectrum for a Spherical Wave

We follow Tatarskii {Eq. (25) on p. 185 in [3]} and denote with α the AOA retrieved from the instantaneous phase difference measured with a two-point interferometer with a baseline b. In our experiments we use small krypton flashlight lamps as sources, which have a diameter of about $D_s = 2$ mm. For visible light ($\lambda \approx 5 \times 10^{-7}$ m), this leads to a far-field range of $2D_s^2/\lambda \approx 16$ m. The propagation path length in the experiment described here was 180 m; thus we assume that the unperturbed wave is a spherical wave, not a plane one. (Plane waves are usually assumed for astronomical observations.)

Clifford [5] developed a theoretical model for the frequency spectrum $S_\alpha(f)$ of AOA fluctuations of a spherical wave propagating through locally homogeneous and isotropic turbulence, assuming that α is measured with a two-point interferometer, where the two point receivers are separated by a baseline of length b. Clifford assumed that the transverse component of the wind vector is parallel to the baseline, and he neglected effects of the longitudinal wind. (Effects of longitudinal wind components are known to be small compared with those caused by transverse wind.) The central equation in Clifford's paper is his Eq. (19):

$$W_{\delta S}(f) = 32\pi^2 k^2 \int_0^L \mathrm{d}x \sin^2\left(\frac{\pi b f x}{v_b L}\right) \times \int_{2\pi f/v_b}^{\infty} \mathrm{d}K\, K \Phi_n(K) \frac{1 + \cos\left[\dfrac{K^2 x(L-x)}{kL}\right]}{\sqrt{(Kv_b)^2 - (2\pi f)^2}}, \quad (1)$$

where $W_{\delta S}(f)$ is the interferometric phase-difference frequency spectrum, f is frequency, $k = 2\pi/\lambda$ is the optical wave number, L is the propagation path length, K is the magnitude of the (turbulence) wave vector, and $\Phi_n(K)$ is the three-dimensional wave number spectrum of the refractive-index fluctuations (assuming isotropy at the wave number K). Further assumptions and approximations that Clifford has made for the derivation of Eq. (1) are that Rytov's approximation (the approximation of smooth perturbations) is valid, Taylor's frozen-turbulence hypothesis is valid for the refractive-index fluctuations, and the wind velocity is a deterministic variable.

In his further development, Clifford assumed that v_b and $\Phi_n(K)$ do not vary along the propagation path, but he did not simplify the mathematics by ignoring diffraction effects. In the following, we do the opposite: we will allow v_b and $\Phi_n(K)$ to vary with x, but we will assume that diffraction effects can be neglected.

With $S_\alpha(f)=W_{\delta S}(f)/(kb)^2$, $v_b=v_b(x)$, and $\Phi_n(K)=\Phi_n(K,x)$, Eq. (1) leads to

$$S_\alpha(f) = 32\pi^2 b^{-2}\int_0^L \mathrm{d}x \sin^2\left[\frac{\pi bfx}{v_b(x)L}\right] \times \int_{2\pi f/v_b(x)}^{\infty} \mathrm{d}K\, K\Phi_n(K,x)\frac{1+\cos\left[\frac{K^2x(L-x)}{kL}\right]}{\sqrt{[Kv_b(x)]^2-(2\pi f)^2}}. \tag{2}$$

1. Geometrical-Optics Approximation

The geometrical-optics approximation is valid if diffraction effects can be neglected. This is the case if in Eq. (2) we can approximate

$$\cos\left[\frac{K^2x(L-x)}{kL}\right] \approx 1. \tag{3}$$

This approximation is valid if $K^2x(L-x)/(kL)\ll 1$, which is fulfilled for all $x\in(0,L)$ if $K^2(L/2)(L-L/2)/(kL)\ll 1$, or

$$K \ll 2\sqrt{k/L}. \tag{4}$$

That is, Eq. (3) is valid if refractive-index fluctuations with wavenumber K larger than the Fresnel wavenumber $\sqrt{k/L}$ contribute only a negligible amount to the K integral in Eq. (2). Because $K\Phi_n(K)/\sqrt{(Kv_b)^2-(2\pi f)^2}$ decreases rapidly with increasing K [note that $\Phi_n(K)$ varies like $K^{-11/3}$ in the inertial subrange], this can be safely assumed if the wavenumber $2\pi f/v_b$ (the lower integration limit in the K integral) meets criterion (4), such that

$$2\pi f/v_b \ll 2\sqrt{k/L}. \tag{5}$$

This translates into a criterion for the frequencies f for which the geometrical-optics approximation, Eq. (3), is valid:

$$f \ll \sqrt{\frac{2}{\pi}}\frac{v_b}{\sqrt{\lambda L}}. \tag{6}$$

That is, for frequencies small compared to the Fresnel frequency,

$$f_F = v_b/\sqrt{\lambda L}, \tag{7}$$

we have

$$S_\alpha(f) = 64\pi^2 b^{-2}\int_0^L \mathrm{d}x \sin^2\left[\frac{\pi bfx}{v_b(x)L}\right] \times \int_{2\pi f/v_b(x)}^{\infty} \mathrm{d}K\frac{K\Phi_n(K,x)}{\sqrt{[Kv_b(x)]^2-(2\pi f)^2}}. \tag{8}$$

We insert Tatarskii's inertial-range spectrum

$$\Phi_n(K,x) = c_T C_n^2(x) K^{-11/3} \tag{9}$$

{Eq. (3.24) on p. 48 in [2]}, where

$$c_T = \frac{\sqrt{3}\Gamma(8/3)}{8\pi^2} = 0.03305, \tag{10}$$

is Tatarskii's coefficient, and we introduce the dimensionless integration variable σ,

$$\sigma = \left[\frac{Kv_b(x)}{2\pi f}\right]^2 - 1. \tag{11}$$

Then we can evaluate the K integral exactly and find

$$S_\alpha(f) = \frac{2^{7/3}}{9\pi^{7/6}\Gamma(5/6)} b^{-2} f^{-8/3}\int_0^L C_n^2(x) v_b^{5/3}(x)\sin^2\left[\frac{\pi bfx}{v_b(x)L}\right]\mathrm{d}x, \tag{12}$$

where we have used Eq. (10) and

$$\int_0^\infty \sigma^{-1/2}(1+\sigma)^{-11/6}\mathrm{d}\sigma = \frac{4}{15}\pi^{3/2}\frac{\sqrt{3}}{\Gamma(2/3)\Gamma(5/6)}. \tag{13}$$

[The numerical coefficient in Eq. (12) has the value 0.1305.]

Let us consider the simplest case where C_n^2 and v_b do not vary with x. Then Eq. (12) gives

$$S_\alpha(f) = \frac{2^{4/3}}{9\pi^{7/6}\Gamma(5/6)} C_n^2 v_b^{5/3} L b^{-2} f^{-8/3}\left[1-\frac{\sin(2\pi bf/v_b)}{2\pi bf/v_b}\right], \tag{14}$$

where the numerical coefficient has the value 0.06524. Equation (14) is identical to Clifford's main result, his Eq. (28). [His slightly different coefficient, 0.066, is probably due to rounding errors, and his factor k^2 instead of b^{-2} is due to an erroneous conversion from $W_{\delta S}(f)$ to $S_\alpha(f)$.] It is quite remarkable that Eq. (14) can be easily obtained via the geometrical-optics approximation, Eq. (3), without the cumbersome integrations that Clifford had to carry out because he did not approximate the cosine term as a constant.

For frequencies large compared with the Fresnel frequency $v_b/\sqrt{\lambda L}$, the cosine term in Eq. (1) oscillates rapidly between −1 and 1, such that the contribution to the K integral becomes negligible. As a result, for $f\gg v_b/\sqrt{\lambda L}$, the magnitude of $S_\alpha(f)$ is, compared with Eq. (14), reduced by a factor of 2, in agreement with Eq. (27) in [5]. This factor of 2 is also consistent with Tatarskii's result {Eqs. (20) and (21) on p. 289 in [3]} that the AOA variance observed with a large-aperture telescope (aperture diameter $D\gg\sqrt{\lambda L}$) is twice the AOA variance observed with a small-aperture telescope ($D\ll\sqrt{\lambda L}$). In their recent analysis based on the Rytov approximation, Cheon and Muschinski [9] showed that the large-aperture asymptote of the circular-aperture AOA variance is reached within 1% for plane waves if $D>1.65\sqrt{\lambda L}$ and for spherical waves if $D>1.84\sqrt{\lambda L}$.

2. Knee Frequency

Let us evaluate Eq. (14) further, with the goal of using it as the model to extract v_b from measured $S_\alpha(f)$. For $2\pi bf/v_b \gg 1$, or

$$f \gg \frac{1}{2\pi}\frac{v_b}{b}, \tag{15}$$

the second term in the square brackets of Eq. (14) can be neglected, and we have

$$S_\alpha(f) = 0.06524 C_n^2 v_b^{5/3} L b^{-2} f^{-8/3}. \tag{16}$$

For $2\pi bf/v_b \ll 1$, however, we can expand the sine function up to third order, $\sin\varphi \approx \varphi - \varphi^3/6$, and we obtain

$$S_\alpha(f) = 0.06524 \frac{2}{3}\pi^2 C_n^2 v_b^{-1/3} L f^{-2/3}. \tag{17}$$

The high-frequency $f^{-8/3}$ asymptote and the low-frequency $f^{-2/3}$ asymptote intersect at the knee frequency,

$$f_k = \frac{\sqrt{6}}{2\pi}\frac{v_b}{b}, \tag{18}$$

or $f_k = 0.39 v_b/b$. If the baseline length b [or an effective baseline, since we retrieve $S_\alpha(f)$ from filled-aperture centroids] is known, then v_b can be retrieved from a measurement of f_k. On the other hand, if both f_k and v_b are measured, then Eq. (18) allows us to determine the effective baseline length empirically. This baseline calibration is necessary if $S_\alpha(f)$ is measured with an instrument that is not a two-point interferometer (as in our case) or if the path-transverse wind component is not parallel to the interferometer baseline.

3. Frequency Dependence of Path-Weighting Functions

According to Eq. (12), the path-weighting function for $S_\alpha(f)$ in the case of a spherical wave is given by

$$W_p(f,x) = C_n^2(x) v_b^{5/3}(x) \sin^2\left[\frac{\pi b f x}{v_b(x) L}\right]. \tag{19}$$

If wind speed and turbulence are homogeneous, then the path-weighting is purely geometric:

$$W_g(f,x) = \sin^2\left(\frac{\pi b f x}{v_b L}\right). \tag{20}$$

It is important to note that $W_g(f,x)$ is frequency dependent. For $\varphi < \pi/4$, the small-angle approximation $\sin\varphi \approx \varphi$ is accurate within 11%, and $\sin^2\varphi \approx \varphi^2$ is accurate within 23%, such that $W_g(f,x)$ varies approximately like x^2 within $(0,L)$ for $\pi b f x/(v_b L) < \pi/4$, or

$$f < \frac{1}{4}\frac{v_b}{b}. \tag{21}$$

That is, for frequencies smaller than the knee frequency, the centroid of $W_p(f,x)$,

$$x_c(f) = \frac{\int_0^L W_g(f,x) x \mathrm{d}x}{\int_0^L W_g(f,x)\mathrm{d}x}, \tag{22}$$

is independent of f and approaches the value $x_c = (3/4)L$, that is, about $L/4$ away from the receiver. For frequencies large compared with f_k, $W_p(f,x)$ oscillates rapidly between 0 and 1, such that the path weighting is practically uniform. The first null in $W_p(f,x)$ within the propagation path, i.e., for $x \in (0,L)$, appears at the frequency

$$f = \frac{1}{\pi}\frac{v_b}{b} = 0.81 f_k. \tag{23}$$

4. Effects of Variability of v_b and C_n^2 on AOA Spectra

The path-weighting becomes more complicated when v_b and C_n^2 vary along the path. The atmospheric weighting function

$$W_a(x) = C_n^2(x) v_b^{5/3}(x), \tag{24}$$

leads to higher contributions to $S_\alpha(f)$ from locations x where C_n^2 and v_b are large. While C_n^2 enters linearly into $W_a(x)$, the baseline wind speed v_b enters with the power of 5/3. The effect of wind-speed variability on the magnitude of $S_\alpha(f)$, however, is almost compensated because v_b enters as v_b^{-2} through the geometric weighting (as long as f is not too large), such that the effect of inhomogeneous wind speed on the AOA spectral density is expected to be small compared with effects of inhomogeneous C_n^2. The main effect of a varying wind speed, regardless of whether within the path or during the observation time during which an estimate of $S_\alpha(f)$ is taken, is that there is a distribution of knee frequencies, such that the sudden drop of $S_\alpha(f)$ is smeared over a certain range of frequencies.

One could approach the problem in a probabilistic fashion: if one allows C_n^2 and v_b to vary randomly, such that $p(C_n^2, v_b)$ is their joint probability density function, then the expected AOA spectrum is

$$\langle S_\alpha(f)\rangle = \int\int p(C_n^2, v_b) S_\alpha(f; C_n^2, v_b)\mathrm{d}C_n^2 \mathrm{d}v_b, \tag{25}$$

where $S_\alpha(f; C_n^2, v_b)$ is given, say, by Eq. (14). An investigation along these lines, however, is beyond the scope of this paper.

B. Interferometric versus Filled-Aperture AOAs

We come back to the question of whether Clifford's [5] interferometric model for spherical-wave AOAs is adequate for interpreting AOAs retrieved from circular-aperture centroids.

Hogge and Butts [10] carried Clifford's analysis further and derived a theoretical model for the frequency spectrum of wavefront tilts over a filled, circular aperture. They expanded the wavefront aberration into Zernike polynomials and found −2/3 and −11/3 asymptotes for frequencies smaller and larger than v/D, respectively, where v is the cross-wind speed and D is the aperture di-

ameter. Along the lines of the remarks by Lawrence and Strohbehn [8] quoted at the beginning of this Section, Hogge and Butts (p. 148 in [10]) offer an interpretation of the steeper asymptote (as compared with the $f^{-8/3}$ laws derived by Tatarskii [3] for plane waves and by Clifford for spherical waves): "The different dependence on frequency we believe can be explained in the following way. For the phase difference spectrum, one measures the difference between the phase fluctuations at precisely two points in space. The phase fluctuations at each point have a power spectrum that varies for large f like $f^{-8/3}$. Hence, the phase difference power spectrum for the higher frequency components (i.e., for those phase fluctuations with scale sizes smaller than the separation of the two measuring points) will also vary as $f^{-8/3}$. On the other hand, the angle-of-arrival power spectra obtained from a least squares fit to the phase distortions is obtained by performing a spatial averaging over the fluctuations in the collecting aperture. Thus, even though distinct points in the field of the collecting aperture may have phase fluctuations that behave as $f^{-8/3}$, the averaged wavefront tilt will not contain as much power at the higher frequencies, and hence, varies for large f as $f^{-11/3}$." However, while Hogge and Butts's explanation helps to understand why centroid-derived AOAs (observed with an aperture of diameter D) have a somewhat smaller *variance* than AOAs obtained from a two-point interferometer with baseline $b=D$, it leaves it unclear why aperture averaging should lead to a *spectral density* with an $f^{-11/3}$ law, as opposed to a different power law or an unchanged ($f^{-8/3}$, say) power law with just a smaller constant of proportionality.

Here we offer a simple physical explanation of the $f^{-11/3}$ law. Consider the interferometric AOA variance $S_\alpha^I(f)qf$ contained in some frequency band around f with a relative width q (1/2, say). Then, according to Taylor's frozen-turbulence hypothesis, $l=v_b/f$ is the transverse scale size of the refractive-index perturbations associated with the AOA fluctuations at frequency f, where v_b is the baseline wind speed. Therefore, the number of independent events (eddies) of size l along a line across the aperture is $N \sim D/l \sim Df/v_b$. According to the law of large numbers, averaging over N independent events reduces the variance by the factor N, and we obtain $S_\alpha^{FA}(f) \sim S_\alpha^I(f)/N \sim (v/D)S_\alpha^I(f)f^{-1}$, where $S_\alpha^{FA}(f)$ is the AOA spectrum obtained with a filled aperture. This, with Eq. (16), leads to

$$S_\alpha^{FA}(f) \sim D^{-3}LC_n^2 v_b^{8/3} f^{-11/3}. \tag{26}$$

This result is consistent with Tyler's result {Eq. (48) in [11]; note that $v=v_b/D$ in Tyler's notation}, who worked out the circular-aperture AOA spectrum for plane waves. (The same result, but with a different numerical coefficient, should follow from Hogge and Butts's spherical-wave theory [10].)

Interestingly, there has been very little observational support for the $f^{-11/3}$ law in the published literature. One reason is that most AOA measurements have been made with interferometric configurations, and those measurements are usually consistent with an $f^{-8/3}$ law (see, e.g., Fig. 64 on p. 305 in [3]; Fig. 4 in [5]; Fig. 3 in [7]), in agreement with theory. The two reports on observations of centroid-derived AOA spectra that we are aware of are somewhat contradictory: Acton *et al.* [12] observed wavefront tilt power spectra from the image motion of solar pores. They write, "Between 5 and 150 Hz, the slopes are approximately −2.6. This is not consistent with either of the theoretical predictions. It is interesting to note, however, that both the measurements of −0.5 and −2.6 are consistent with the slope predictions of −2/3 (low) and −8/3 (high) for a phase-difference power spectrum. Tatarskii also derived the phase-difference PSD slopes and then stated without proof that the same slopes should be applicable to a wave-front tilt PSD." On the other hand, more recent observations by McGaughey and Aitken [13] do support an $f^{-11/3}$ power law (Fig. 3 in [13]). McGaughey and Aitken point out that "the expected −11/3 index is evident only when the estimated noise level is subtracted from the curves."

3. EXPERIMENT

Field experiments were conducted after sunset on September 27 and 28, 2006, at BAO near Erie, Colorado. The BAO is a research facility operated by NOAA (the National Oceanic and Atmospheric Administration) with the purpose of facilitating investigations of the atmospheric boundary layer. The primary feature of the BAO facility is a 300 m tower erected over wide open and reasonably flat terrain [14,15]. All instruments were set up at the southeast side of the BAO tower, as shown in Fig. 1. The ground cover surrounding the experiment site was uniform in all directions and consisted of dry brush with a height of 30 to 90 cm as shown in Fig. 2.

A. Experimental Setup

A large-aperture telescope (Model LX200GPS, Schmidt–Cassegrain type, manufactured by Meade Instruments Corporation of Irvine, California) was set up approximately 100 m from the BAO tower, and the legs of the telescope frame adjusted such that the center of the aperture was 1.5 m above ground level (AGL). Four krypton flashlight bulbs, each with an aperture diameter of ~2 mm, were arranged on a sturdy metal tripod that was positioned 180 m southeast of the telescope (bearing of 140.8 deg relative to North). The individual bulbs were arranged at the corners of a rectangle with a spacing of 10 cm in the horizontal and 9 cm in the vertical. The center of the array of bulbs was at 0.94 m AGL.

After the telescope was focused, a black-and-white CCD camera (Model 075M, manufactured by Lumenera Corporation of Ottawa, Ontario, Canada) was mounted at the rear-side observation port of the telescope. A laptop computer with an external hard disk drive was connected to the CCD camera and ran software that controlled the parameters associated with image capture (i.e., frame rate and exposure time; see Subsection 3.B for more detail).

An ultrasonic anemometer–thermometer (Model 81000, manufactured by R. M. Young Company of Traverse City, Michigan), from this point onward referred to as the "sonic," was set up at 64 m from the telescope along the line of the optical propagation path at a height of 1.5 m AGL and within 1 m of the propagation path hori-

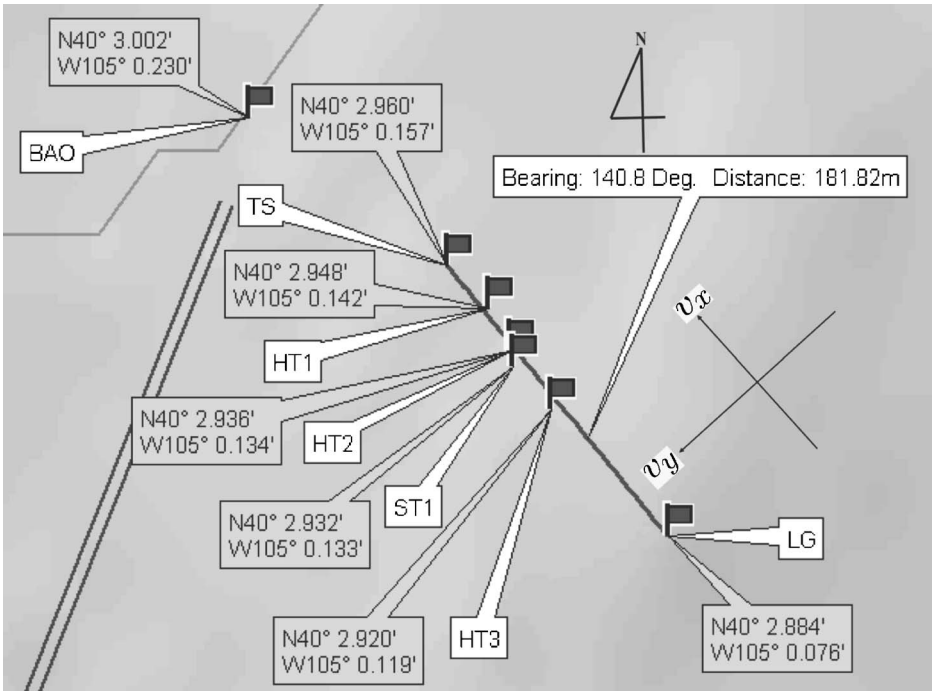

Fig. 1. Diagram of position of the instruments and the propagation path at Boulder Atmospheric Observatory (BAO) near Erie, Colorado, generated from DeLorme Topo USA 3.0. BAO, BAO tower; TS, telescope; HT and ST, self-logging thermometer towers and ultrasonic anemometer tower, respectively; LG, light.

Fig. 2. Experimental setup with the 14-in. telescope, ultrasonic anemometer, and self-logging thermometers at BAO.

zontally. The sonic measured three components of the local, instantaneous wind velocity, which we call v_x, v_y, and v_z (see Subsection 5.B).

Fifteen self-logging, thermistor-based thermometers (Model HOBO H8 Pro, manufactured by Onset Computer Corporation of Pocasset, Massachusetts) were deployed in three vertical arrays (of five sensors each) that were positioned 31, 56, and 94 m from the telescope, along the optical propagation path. Each array of five sensors was mounted securely to a stable stand (photographic light stand with tripod legs). The sensors were spaced vertically along each stand at heights 0.3, 0.5, 1.0, 1.5, and 2.0 m AGL.

B. Technical Details and Operation of Instruments

The telescope was of the Schmidt–Cassegrain type. That is, its physical aperture area was annular such that light arriving at the aperture entered the telescope through a region concentric about a circular, center obstruction. The aperture had a 36 cm outer diameter, and the center obstruction had a diameter of 12.7 cm. The focal length, F, of the telescope was 3556 mm. The angular resolution of the telescope was, according to the Rayleigh criterion {Eq. (1) in [16]}, $1.22\lambda/D = 1.71\ \mu\text{rad} = 0.35$ arcsec for $\lambda = 500$ nm. The telescope was focused on the bulb array and the CCD camera attached as discussed above. The telescope adjustment remained fixed for the duration of each experiment.

The CCD camera had 640×480 pixels, and the spacing between each pixel was 7.4 μm in both directions, translating to an AOA increment of 2.08 μrad per pixel. The peak sensitivity of the CCD was to wavelengths of 500 nm. The camera was controlled by a laptop computer which ran software (Stream Pix, Version 3.21.0) that specified the number of pixels, the exposure time, the frame rate, and the bit depth. The number of pixels was 640×480 pixels. The exposure time of the CCD camera was set to 35 μs (from an available range of 1 μs to 400 s), which was determined as the optimal value to maximize the signal-to-noise ratio and yet avoid saturation. The frame rate was set to 30 frames/s, which was found to be the maximum frame rate for which all frames could be reliably saved. The bit depth was set to 12 bits.

The image data, saved in an external hard disk drive, were given individual time stamps that were extracted from the system clock of the computer. The system clock was manually synchronized with that of the data-logging system (developed by the authors M. Behn and A. Muschinski) for the sonic, to ensure consistency of time-series data between the two instruments with an accuracy of about 1 s.

The sonic, at the setting used for the present experiments, had a measurable wind speed range from 0 to 40 m s^{-1} with a resolution of 0.01 m s^{-1} and a measurable temperature range from −50 to +50°C with a resolution of 0.01°C. The sampling rate was adjustable within the range 0–32 Hz, of which only the maximum 32 Hz was used. The data were saved in a local storage of the data-logging system. A time stamp was provided for each data point by means of a GPS (Global Positioning System) receiver, which automated the synchronization of the on-board system clock of the data-logging system with a GPS clock.

The self-logging thermometers were rated to measure temperature in the range −30–50°C with an accuracy of ±0.2°C at 25°C. The sampling period of 5 s was used (from an available range of 0.5 s to 9 h), and all data were stored in the on-board memory. As with the CCD camera, the internal clock of each temperature sensor was synchronized with that of the data-logging unit for the sonic, to maintain consistency in time between all data sources.

Utilizing the instruments as described above, CCD images of the bulb array along with supporting wind and temperature information from the sonic and self-logging thermometers were collected in two approximately 1 h intervals, the first between 21:00 and 22:00 on September 27, 2006, and the second between 18:00 and 19:00 on September 28, 2006. Processing of the data and experimental results of the first data set are presented in the sections that follow.

4. DATA PROCESSING

In this section, we describe a procedure to estimate wind speeds from digital images of a point source. We proceed in three steps: first, time series of vertical and horizontal AOAs are estimated from the sequences of digital images; second, we estimate three parameters (C_n^2, the model baseline wind speed $\tilde{v}_b$, and a noise floor) in Clifford's model for the AOA frequency spectrum by fitting the model spectrum to the observed AOA spectra; third, we retrieve the calibrated baseline wind speed v_{aoa}^c, assuming a linear relationship between $\tilde{v}_b$ and v_{aoa}^c.

A. Estimating Image Centroids and AOAs

The digital images are discrete-time sequences of the intensity field measured in the focal plane. Assuming that the telescope is focused on a point source and neglecting diffraction effects due to the finite size of the aperture [16], a spherical wave emitted from the source would be observed as a point image, whose pixel coordinates i and j lead to the AOAs

$$\begin{pmatrix} \alpha_y \\ \alpha_z \end{pmatrix} = \frac{1}{F}\begin{pmatrix} \Delta_y i \\ \Delta_z j \end{pmatrix} = \begin{pmatrix} \Delta\alpha_y i \\ \Delta\alpha_z j \end{pmatrix}, \tag{27}$$

where F is the focal length, and Δ_y and Δ_z are the physical pixel spacings in the horizontal and vertical direction, respectively. In our case, $\Delta_y=\Delta_z=7.4\ \mu$m and $F=3.556$ m, which gives the angular pixel resolutions $\Delta\alpha_y=\Delta\alpha_z=2.08\ \mu$rad.

However, turbulent refractive-index perturbations along the propagation path lead to phase-front distortions, causing local, instantaneous AOAs to vary across the aperture and resulting in a blurred image. According to Gurvich and Kallistratova [17], the instantaneous AOA centroids $\bar{\alpha}_y$ and $\bar{\alpha}_z$,

$$\begin{pmatrix} \bar{\alpha}_y \\ \bar{\alpha}_z \end{pmatrix} = \frac{\sum_{i,j}\begin{pmatrix} \Delta\alpha_y i \\ \Delta\alpha_z j \end{pmatrix} I_{ij}}{\sum_{i,j} I_{ij}}, \tag{28}$$

may be used as aperture-averaged AOAs.

For calibration of CCD images (p. 157 in [18]), a master dark image (average of dark images) can be used to remove a dark current caused by thermal noise. Both before and after recording light images, dark images were recorded by covering the aperture of the telescope. After removing the dark current by subtracting the master dark image, we divided images into four sections, one for each of the four light sources, and each section was centered with the maximum intensity of each light. The diameters of the (blurred) images were about 30 pixels, that is, about 60 μrad. Howell (p. 181 in [19]) claimed that in order to determine the mean of the background intensity, the size of the image should be about three times the size of the spot. Thus, we chose a section size of 101×101 pixels. We subtracted the mean background intensity for each section, which was calculated after the bright spot was excluded. Then, we calculated the aperture-averaged AOAs by using Eq. (28).

B. Least-Squares Optimization

The frequency spectrum of the AOA fluctuations, as shown in Eq. (14), is a function of the refractive-index structure constant, C_n^2, and the transverse wind speed, $\tilde{v}_b$, for the given propagation distance, L, and baseline, b, for the interferometer or aperture size, D, for the telescope. The frequency spectrum that is distinct enough to easily define the knee frequency might not always be obtained because of intermittency of turbulence or the presence of a high noise floor. Thus, it is necessary to have a systematic way for retrieving the knee frequency or the transverse wind speed. We used Eq. (14) to fit a function to the observed frequency spectrum of AOA fluctuations by a least-squares optimization.

Let $S_{\alpha,i}^m(f,C_n^2,\tilde{v}_b)$ be the observed frequency spectrum and $S_{\alpha,i}^t(f,C_n^2,\tilde{v}_b)$ be the Clifford model. It is necessary to find C_n^2 and $\tilde{v}_b$ (L and D are given) for minimizing a cost function, C, where

$$C = \sum_{i=1}^{N} [\log_{10} S_{\alpha,i}^t(f,C_n^2,\tilde{v}_b) - \log_{10} S_{\alpha,i}^m(f,C_n^2,\tilde{v}_b)]^2, \tag{29}$$

$$S_{\alpha,i}^t(f,C_n^2,\tilde{v}_b) = 0.065C_n^2 L\tilde{v}_b^{5/3}D^{-2}\left[1-\frac{\sin(2\pi Df/\tilde{v}_b)}{2\pi Df/\tilde{v}_b}\right]f^{-8/3} + S_{\mathrm{noise}}, \tag{30}$$

and $f=\{f_1,f_2,\cdots,f_N\}$. Note that we used the aperture diameter D as (a first guess of) the effective baseline b_{eff}. We will determine b_{eff} in terms of D *a posteriori*.

The logarithm of the spectra is taken in the cost function to avoid underevaluation for the high-frequency por-

tion of the spectra. The noise, S_{noise} was added to the Clifford model to take into account the noise floor of the observed frequency spectra. Thus, the variables for the optimization are C_n^2, $\tilde{v}_b$, and S_{noise}. A MATLAB function, fminsearch, was used for the least-squares optimization. To define the frequency range for the optimization, we multiplied $f^{+5/3}$ times the spectrum so that the spectrum is proportional to f^{+1} and f^{-1} for the low- and high-frequency portions, respectively, and obtained f_m, the frequency for the maximum of the f^{+1}/f^{-1} representation. We specified the beginning frequency, f_1 for the optimization as f_m/M, and $M=9$ was chosen to obtain the minimum rms difference between the transverse wind speed retrieved from the frequency spectra and the transverse wind speed measured by the sonic (discussed further in Section 5). The end frequency f_N was specified as the Nyquist frequency.

C. Calibration of Transverse Wind Speed

Let us designate $f_k=0.39\tilde{v}_b/b$ as the knee frequency retrieved from the spectrum of AOA fluctuations and v_b as the time-averaged transverse wind speed measured by the sonic. To calibrate the transverse wind speed, we compared f_k with v_b by plotting a scatter plot and obtained a calibration line, $f_k=p_1v_b+p_0$, by interpolating the data set. The y intercept, p_0 (zero-mean wind offset, ideally $p_0=0$) was added to account for the fluctuations of the transverse mean wind speed. To eliminate the effect of outliers on the calibration, we calculated the standard deviation, σ_d of the distance between each data point and the calibration line and removed the data outside the bound of $\pm 2\sigma_d$. Then, we calculated a new calibration line, and the transverse wind speed can be calibrated as

$$v_{\text{aoa}}^c = \frac{bf_k/0.39 - p_0}{p_1}. \tag{31}$$

5. RESULTS AND DISCUSSION

As mentioned in Section 3, four krypton flashlight bulbs (two bottom lights and two top lights) were used as sources. In this paper, only the AOAs and the frequency spectra of AOA fluctuations from the bottom lights (as viewed from the telescope) were analyzed. Analysis for multiple lights will be the subject of future work.

A. Angle-of-Arrival

Figure 3 shows an image of the four lights measured at 21:00:10 LT (local time), September 27, 2006. The intensity of light in the image is linear in scale, and the maximum value of the intensity is 1529 ADU (analog-to-digital unit) at a pixel location (horizontal, vertical) of (177, 374), which corresponds to the bottom left-hand light. The mean of the intensity over the entire image is 3.3 ADU, and the intensity of the background is in the range of 0 to 15 ADU. The ratio of the maximum intensity of the light with the maximum intensity of the background is 46 dB. Figure 4 shows 20 images of the bottom left-hand light, each with a size of 51×51 in pixel number. The intensity fluctuations and blurring of the light images are evident.

The centroids for the horizontal and vertical directions (in pixel number) were obtained, and the horizontal and vertical AOAs, $\bar{\alpha}_y$ and $\bar{\alpha}_z$, of the bottom left-hand light were calculated as discussed previously. Figure 5 shows the AOAs for (a) the horizontal direction and (b) the vertical direction for the bottom left-hand light measured on September 27, 2006. The means are subtracted for both directions. The standard deviations for $\bar{\alpha}_y$ and $\bar{\alpha}_z$ are 5.44 and 27.49 μrad, respectively.

At night, it can be assumed that the atmosphere is stratified parallel to the ground and that the vertical temperature gradient is dominant compared with the horizontal. Furthermore, the temperature near the ground decreases more rapidly than that at a certain height, and

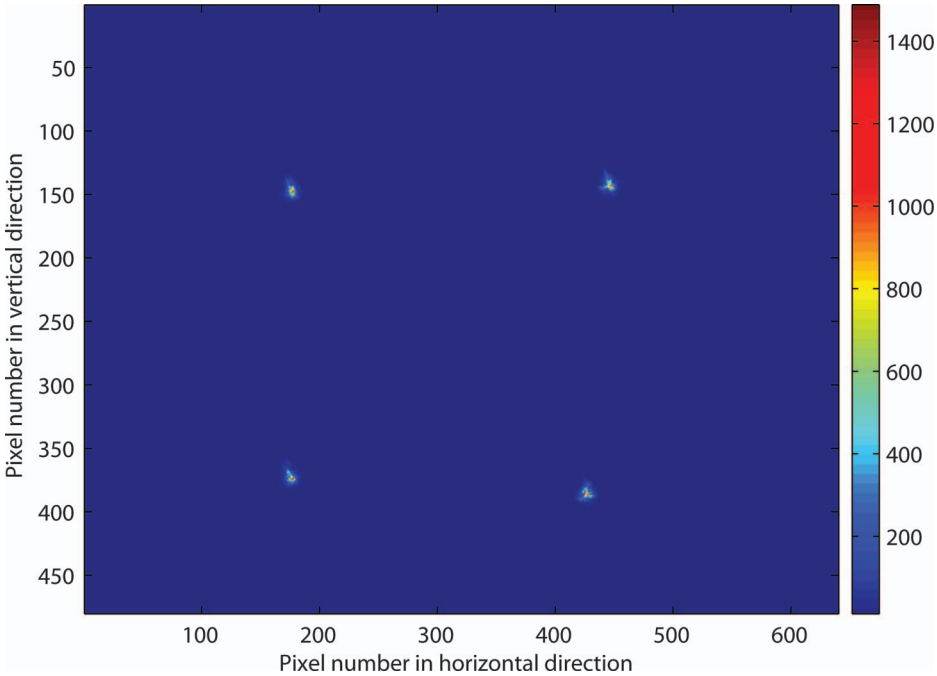

Fig. 3. Image of four lights measured at 21:00:10 LT, September 27, 2006.

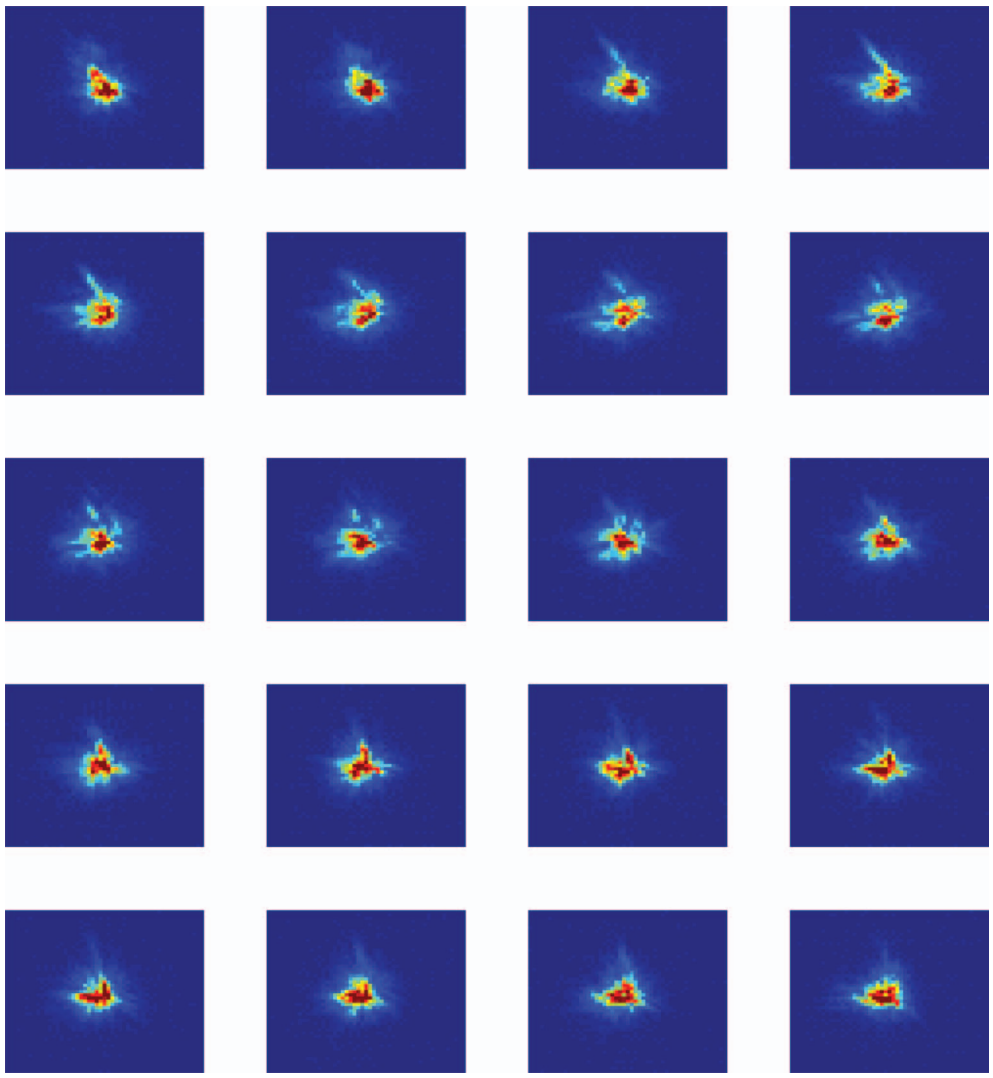

Fig. 4. Sequence of subimages (51×51 pixels) of the bottom left-hand light, measured at 21:00:10.9–21:00:11.6 LT, September 27, 2006. The first row, first column is the first image, the first row, fourth column is the fourth image.

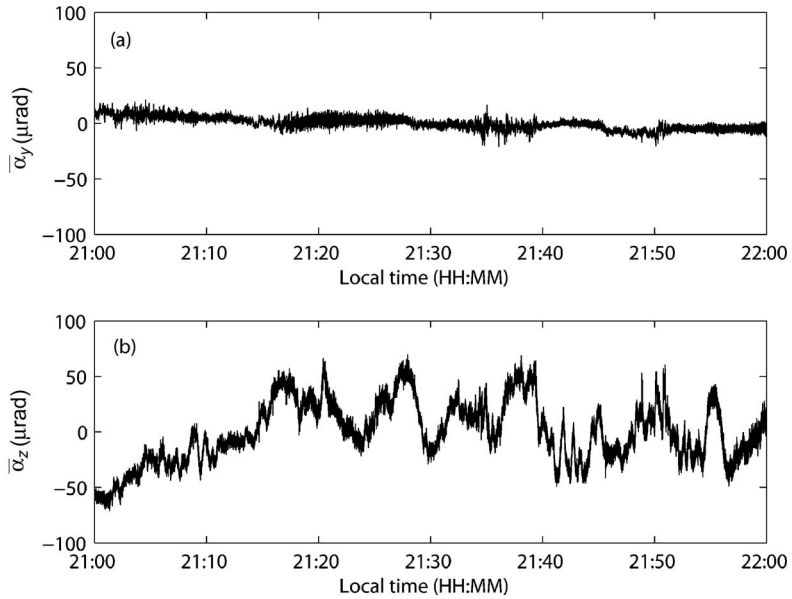

Fig. 5. AOA time series for (a) the horizontal direction and (b) the vertical direction of the bottom left-hand light measured on September 27, 2006.

the mean vertical temperature gradient is positive. Thus, rays of the optical wave in the current setup bend downward at the aperture of the telescope, and the apparent position of the light is therefore higher than the real position of the light. The higher temperature gradient we have, the higher $\bar{\alpha}_z$ we have. Figure 6 shows $\bar{\alpha}_z$ of the bottom left-hand light and the vertical temperature gradient between 1 and 2 m (recall that the optical propagation path is 1.5 m AGL) measured by the middle array of self-logging thermometers (56 m from the telescope). The mean and standard deviation of the vertical temperature gradient were 0.89 K m^{-1} and 0.27 K m^{-1}, respectively. It was observed that if the vertical temperature gradient increases, $\bar{\alpha}_z$ increases, and if the vertical temperature gradient decreases, $\bar{\alpha}_z$ decreases. The correlation coefficient between $\bar{\alpha}_z$ and the vertical temperature gradient was found to be 0.8.

B. Wind Speed

We defined v_x as the wind speed along the optical propagation path and v_y and v_z as the wind speeds perpendicular to the propagation path. Wind blowing from the lights to the telescope is denoted $+v_x$, wind blowing from right to left viewed from the light (as shown in Fig. 1) is denoted $+v_y$, and wind blowing upward from ground is denoted $+v_z$. The transverse horizontal wind speed, $v_b=|v_y|$, with 30 s averaging time, is shown in Fig. 10 below (solid curve in top panel), and the mean and standard deviations of v_b, were 0.37 and 0.18 m s^{-1}, respectively.

C. Frequency Spectrum of AOA Fluctuations

The frequency spectra of AOA fluctuations were obtained by taking the Fourier transform of the time series of AOA fluctuations. Figure 7 shows the averaged frequency spectra of 12 frequency spectra of AOA fluctuations (each spectrum was obtained for 10 s of time duration) and frequency spectra averaged over intervals of equal logarithmic width for 2 min of time duration for the horizontal and vertical directions. The observation time was 21:20:10 to 21:22:10 LT, September 27, 2006. During the observation time, the mean of the transverse horizontal wind speed, v_b, was 0.74 m s^{-1}.

From Fig. 7, there appears to be three distinct regimes of the spectra for the horizontal AOA fluctuations: a low-frequency band, $f<0.3$ Hz; a mid-range band, $0.3<f<2$ Hz; and a high-frequency band, $f>2$ Hz. The previously defined knee frequency is the intersection between the mid-range and high-frequency bands. For the horizontal direction, the knee frequency is ~2 Hz, and the frequency spectrum is proportional to $f^{-2/3}$ for frequencies smaller than the knee frequency, but is above the low cutoff at 0.3 Hz and $f^{-8/3}$ for frequencies larger than the knee frequency.

Below 0.3 Hz, the frequency spectrum for the horizontal direction is divergent from the −2/3 power law and smaller than that for the vertical direction, which corresponds to the outer scale of turbulence that is of the order of meters. Lüdi and Magun [7] observed that the frequency spectrum of the horizontal AOA fluctuations is smaller than that of the vertical AOA fluctuations in the low-frequency band with a larger outer scale of turbulence in the horizontal direction than in the vertical direction for a stable and stratified atmosphere; this is similar to our result. This result is understandable given that the AOAs are the aperture-averaged phase differences over the aperture and that inhomogeneities cross the beam of the wave. When the outer scale of the turbulence in the horizontal direction is larger than in the vertical direction, the spatial correlation length for the horizontal direction is larger than that for the vertical direction. The phase difference in the horizontal direction is smaller than that in the vertical direction.

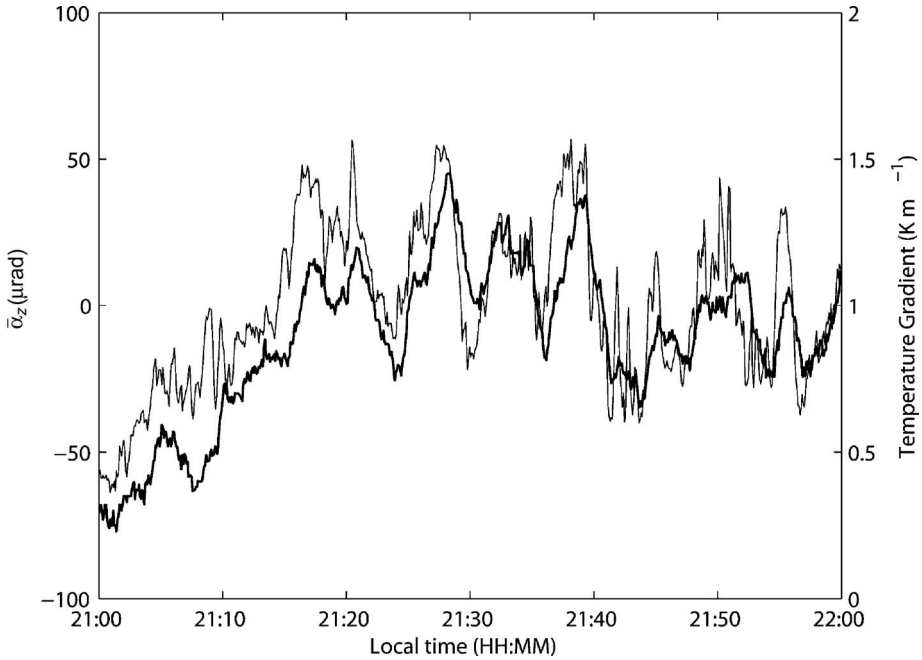

Fig. 6. Vertical AOA, $\bar{\alpha}_z$ (thin curve) of the bottom left-hand light and the vertical temperature gradient (thick curve) between 1 and 2 m measured by the self-logging thermometers at 56 m from the telescope with 5 s averaging time measured on September 27, 2006.

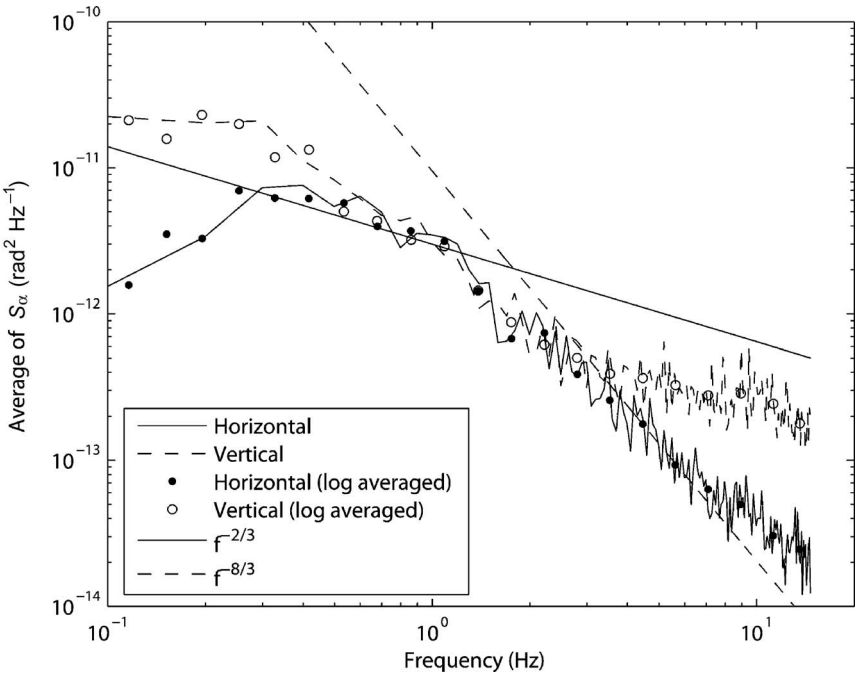

Fig. 7. Averaged frequency spectra of AOA fluctuations for the horizontal direction (solid line) and the vertical direction (dashed line) of the bottom left-hand light measured on September 27, 2006. Each spectrum is for 10 s of time duration. The black dots and open circles are the frequency spectra averaged over intervals of equal logarithmic width for horizontal and vertical directions of 2 min of time duration, respectively. The observation time was 21:20:10–21:22:10 LT.

For $f > 5$ Hz, the frequency spectrum for the vertical direction deviated from the $-8/3$ power law because of noise contamination, which may be due to mechanical vibrations caused by wind passing over the telescope housing. Figure 2 shows the telescope mounting, which is clearly more susceptible to vibration in the vertical (due to the bearing on which it pivots) than in the horizontal direction. The telescope vibrations can cause a spike in the frequency spectrum [20], which is not distinctive in our experiment. The standard deviations of the noise were ~ 0.7 and ~ 2 μrad for the horizontal and vertical directions, respectively.

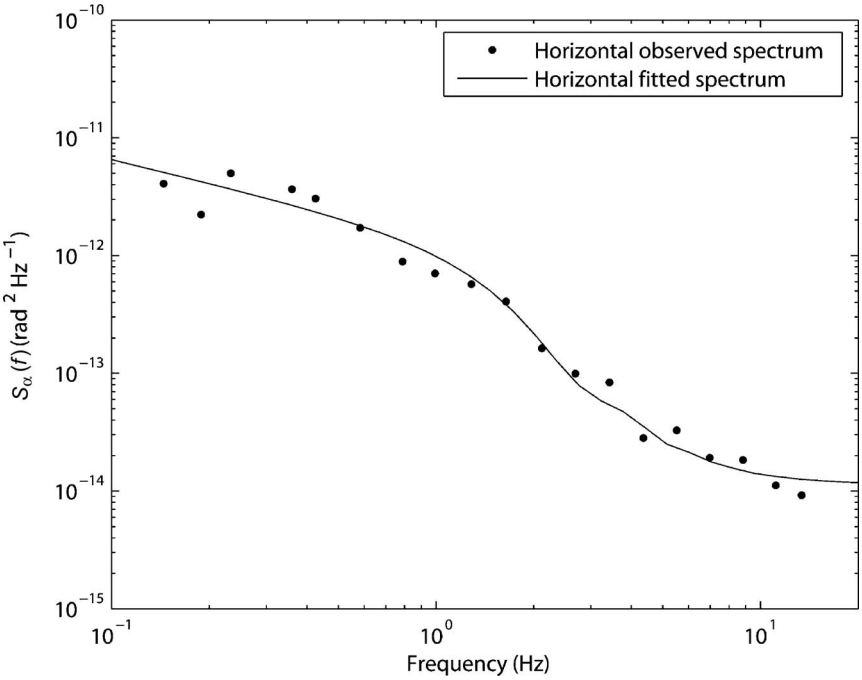

Fig. 8. Averaged over logarithmically equidistant steps, observed and fitted frequency spectra of horizontal AOA fluctuations of the bottom left-hand light measured on September 27, 2006. The observation time was 21:06:10–21:06:40 LT. The dots are for the observed spectrum, and the solid curve is for the fitted spectrum.

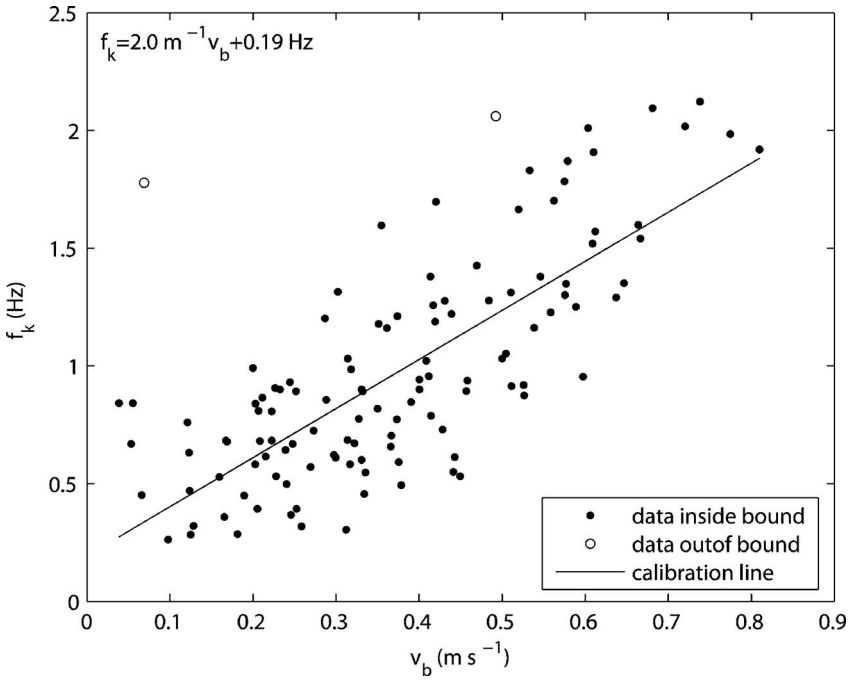

Fig. 9. Scatter plot of the knee frequency, f_k, from the frequency spectra of horizontal AOA fluctuations (bottom left-hand light) versus the time-averaged transverse horizontal wind speed measured by the ultrasonic anemometer, v_b, measured on September 27, 2006. The dots are the data inside the bound ($\pm 2\sigma_d$), the open circles are the data out of the bound, and the solid line is the calibration line. The calibration line is $f_k = 2.0\ \mathrm{m}^{-1} \times v_b + 0.19\ \mathrm{Hz}$. The averaging time is 30 s.

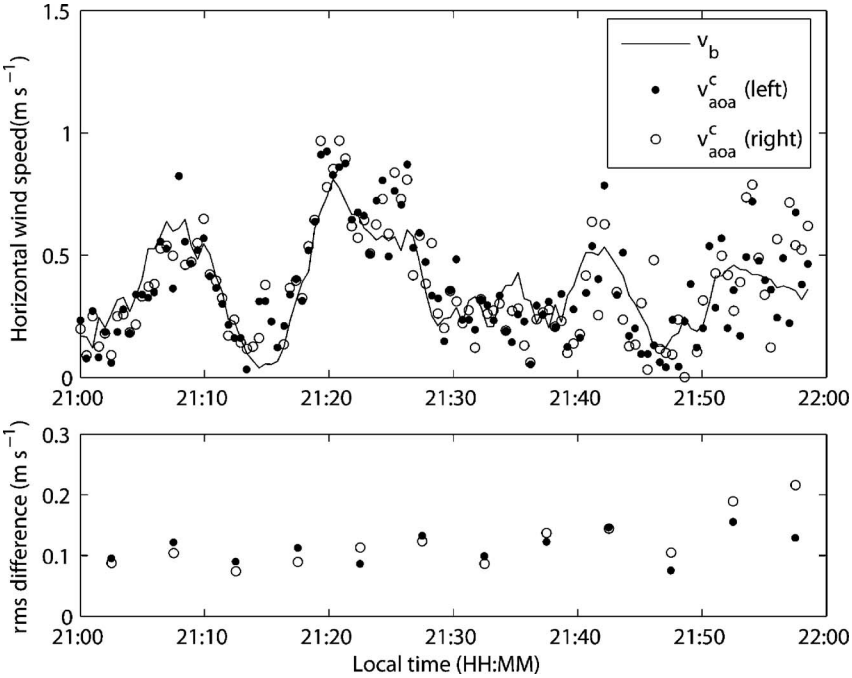

Fig. 10. Comparison of v^c_{aoa} with v_b (top panel) and rms difference between v^c_{aoa} and v_b (bottom panel) measured on September 27, 2006. The solid curve is for the 30 s averaged transverse horizontal wind speed measured by the ultrasonic anemometer. The filled and open circles (top panel) are for the calibrated path-averaged transverse horizontal wind speeds retrieved from the frequency spectra of the horizontal AOAs fluctuations for 30 s of time duration for the bottom left-hand and bottom right-hand lights as viewed from the telescope, respectively. The filled and open circles (bottom panel) show the rms difference between v^c_{aoa} and v_b for the bottom left- and right-hand lights for 5 min of averaging time, respectively.

D. Comparison of f_k with v_b

Once the frequency spectrum of the horizontal AOA fluctuations was obtained, the frequency spectrum was fitted by using the Clifford model by least-squares optimization to obtain the refractive-index structure constant, C_n^2, the path-averaged transverse horizontal wind speed, v_{aoa}, and the level of noise floor, S_{noise} with 30 s intervals. Figure 8 shows the observed (bottom left-hand light) and fitted frequency spectra of AOA fluctuations for the horizontal direction for the observation time of 21:06:10 to 21:06:40 LT, September 27, 2006. During the observation time, the mean and standard deviation of the transverse horizontal wind speed, v_s, were 0.51 and 0.06 m s^{-1}, respectively. The fitted frequency spectrum obtained by least-squares optimization follows the observed frequency spectrum very well, and the knee frequency $f_k = 0.91$ Hz was obtained.

A calibration line was obtained from the comparison of f_k with v_b. For 30 s averaging time, the calibration line was $f_k = 1.99\ \mathrm{m}^{-1} \times v_b + 0.25$ Hz. Then, the standard deviation of the distance between each data point and the calibration line, σ_d, was found to be 0.32 Hz. As previously discussed, the data out of the bound $\pm 2\sigma_d$ were removed, and the calibration line was recalculated. Figure 9 shows the scatter plot of f_k (bottom left-hand light) versus v_b after the out-of-bound data (open circle in the figure) were removed for 30 s averaging time. The calibration line was then $f_k = 2.0\ \mathrm{m}^{-1} \times v_b + 0.19$ Hz. For comparison, the same process was performed for 60 s averaging time, and the calibration line was $f_k = 2.0\ \mathrm{m}^{-1} \times v_b + 0.07$ Hz. The correlation coefficients between f_k and the calibration lines were 0.78 and 0.85 for 30 and 60 s averaging times, respectively. We observe in the calibration lines, for both 30 and 60 s of averaging times, two deviations from ideal behavior; a slope >1 and an intercept >0. Both indicate the presence of features in the physical measurement of AOA that are not accounted for in the Clifford model. Some of these are discussed in the following section.

Figure 10 (top) shows the time-averaged transverse horizontal wind speed v_b, with 30 s of averaging time measured by the sonic at 64 m from the telescope, and the calibrated path-averaged transverse horizontal wind speed v_{aoa}^c, from the frequency spectra of horizontal AOA fluctuations from the bottom left- and right-hand lights (as viewed from the telescope) using Eq. (31); v_{aoa}^c agrees with v_b reasonably well. Figure 10 (bottom) shows the rms difference between v_{aoa}^c and v_b for 5 min of averaging time. The rms differences for both lights are increased significantly after 21:50 LT, which might be caused by a low signal-to-noise ratio. The ratio between the maximum intensity of light and the maximum background intensity was $\sim 2/3$ of that at the beginning of experiment. For the bottom left-hand light, the mean rms differences between v_{aoa}^c and v_b are 11 cm s^{-1} for 30 s averaging, which is 29% of the mean transverse horizontal wind speed (37 cm s^{-1}), and 8.8 cm s^{-1} for 60 s averaging, which is 23% of the mean transverse horizontal wind speed. For the bottom right-hand light, the mean rms differences are 11 cm s^{-1} (29% of the mean transverse horizontal wind speed) and 9.6 cm s^{-1} (26% of the mean transverse horizontal wind speed) for 30 and 60 s averaging times, respectively. Since v_{aoa}^c is the path-averaged transverse horizontal wind speed and v_b is the time-averaged transverse horizontal wind speed measured at one position, v_{aoa}^c fluctuates more than v_s; the standard deviations of v_{aoa}^c are 0.22 m s^{-1} for the bottom left- and right-hand lights, and the standard deviation of v_s is 0.17 m s^{-1}.

E. Limitations of Applicability of Theoretical Models

On the one hand, we have shown that there is a high correlation between the retrievals of f_k and the independent measurements of v_b. On the other hand, there are quite a number of reasons, some of which we list in the following, why it would be unrealistic to expect our data to follow an idealized theoretical model precisely, regardless of whether we would have chosen the (perhaps more realistic) Hogge and Butts model [10] instead of Clifford's model [5], or some other model. The point that we want to make is that our method relies on the detectability of the knee, rather than on a precise fitting of our data to a specific model. Theoretical models can be refined in several respects, as indicated in the following. Such model improvements, however, may turn out to be of limited value for the improvement of wind retrieval techniques.

1. Extended Source

Our light source was a bulb with a diameter of about 2 mm, corresponding to an angular diameter of about 10 μrad at a range of $L = 180$ m. Therefore, the unperturbed wave was not a spherical one, contrary to our model assumption. Kallistratova and Kon [21] studied AOA fluctuations of light waves from an extended source. They assumed that each point of the extended source acts as an independent source and then averaged over the different contributions. They showed that if the size of the source is increased by a factor of 30, the knee frequency of the frequency spectrum of AOA fluctuations is decreased by a factor of 10.

2. Anisotropy of Turbulence

All the standard models [3,5,10,11] assume that the turbulence is statistically isotropic. Atmospheric turbulence, however, is rarely isotropic (p. 96 in [22]), particularly in the atmospheric surface layer under clear skies, as in our case. Lee and Harp [23] suggested an *ad hoc* model for anisotropic turbulence, which has been used by various authors mostly because of its mathematical convenience. However, the Lee and Harp anisotropy model is not supported by turbulence theory.

3. Outer-Scale and Inner-Scale Effects

For the sake of mathematical convenience, all standard models assume that the inertial-range turbulence model is valid for all wave numbers over which the K-space integration has to be performed. For the technique described in this paper, it is important that the effective baseline is well within the inertial subrange. This was fulfilled in our measurements, since the height above ground level (which in the atmospheric surface layer sets the outer scale of turbulence) was significantly larger than the effective baseline of 20 cm, and the inner scale close to the ground is typically smaller than 1 cm.

4. Inhomogeneity and Nonstationarity of the Transverse Wind

In all standard models, including the Clifford model, Eq. (14), the transverse horizontal mean wind speed, v_b, is assumed to be homogeneous along the optical propagation path, and fluctuations of the mean wind speed are not taken into account. This assumption is often unrealistic, in particular in complex terrain and in situations where radiative forcing is important, such as in daytime convection and in the nocturnal boundary layer. The probability density function of the cross-wind speed could be taken into account for a more sophisticated model of the frequency spectrum of AOA fluctuations, as mentioned in Subsection 2.A (see also p. 266 in [24]).

6. SUMMARY AND CONCLUSIONS

We have presented measurements of optical angle-of-arrival (AOA) fluctuations along a 180 m long, horizontal propagation path at the Boulder Atmospheric Observatory (BAO) site near Erie, Colorado. The propagation path was 1.5 m above ground level (AGL), and the measurements were taken during a 1 h long period after sunset on a clear, calm, late-September night with strong radiative cooling near the ground. Bright, small krypton flashlight lamps served as light sources. Time series of vertical and horizontal AOAs were retrieved from centroids calculated from digital images (30 images/s) taken with a CCD camera connected to a commercial Schmidt–Cassegrain telescope with an aperture diameter of 36 cm. During the 1 h long observational period, 1 min averages of the cross-path wind (as measured with the sonic) varied between less than 10 cm s^{-1} and ~1 m s^{-1}.

We analyzed frequency spectra $S_\alpha(f)$ of the horizontal AOA fluctuations, with the main goal of exploring the usefulness of cross-path wind-speed retrievals from observations of the knee frequency f_k [the frequency at which the low-frequency $f^{-2/3}$ asymptote of $S_\alpha(f)$ intersects the high-frequency $f^{-8/3}$ asymptote]. High time resolution ultrasonic-anemometer–thermometer ("sonic") measurements of the wind vector were made at a location along the propagation path at the same height (1.5 m AGL). We used Clifford's [5] theoretical model for the AOA spectrum observed with a two-point interferometer (two point receivers separated by a baseline of length b) to derive a relationship between the interferometer baseline length b and the baseline wind (cross-path wind speed in our case) v_b. From Clifford's theory, we find $f_k = 0.39 v_b / b$.

Our main empirical results are the following:

1. Frequency spectra $S_\alpha(f)$ of horizontal AOA fluctuations estimated from periods ranging from a few tens of seconds to a few minutes show fairly consistently a $f^{-2/3}$ regime at lower frequencies and a $f^{-8/3}$ regime at higher frequencies, with f_k of the order of 1 Hz.

2. 30 s estimates of f_k and 30 s averages of v_b are highly correlated, and a linear regression gives the relationship

$$f_k = 2.0\ \mathrm{m^{-1}} \times v_b + 0.19\ \mathrm{Hz}. \tag{32}$$

3. Interpreting the slope of the regression line as $0.39/b_{\mathrm{eff}}$ gives an effective baseline length of $b_{\mathrm{eff}} = 20$ cm, which is about half the physical diameter of the telescope aperture ($D = 36$ cm).

4. Interpreting the zero-wind offset $f_{k0} = 0.19$ Hz as due to an rms value σ_v of a variable cross wind along the path, we obtain $\sigma_v = f_{k0}/(2.0\ \mathrm{m^{-1}}) = 9\ \mathrm{cm\ s^{-1}}$, an amount that is consistent with the rms difference between the *in situ* measured and optically retrieved cross-path wind speeds (see Fig. 10).

On the basis of data collected in a field experiment, we have demonstrated that the knee frequency obtained from horizontal AOA frequency spectra estimated from images taken with a CCD camera mounted on a commercial, large-aperture telescope are useful for the quantitative retrieval of cross-path wind speeds. In our case, the accuracy of the retrieved wind speeds was about 10 cm s^{-1}. This technique relies on the detectability of the predicted rapid dropoff of $S_\alpha(f)$ at $f_k = 0.39 v_b / b_{\mathrm{eff}}$, where b_{eff} is the effective baseline of the optical sensor, in our case a certain fraction of the aperture diameter. In order to retrieve wind speeds quantitatively, b_{eff} has to be calibrated in an experiment where the actual wind speed is measured independently, as described in this paper. For our Schmidt–Cassegrain telescope (36 cm aperture diameter, with a circular, central obstruction of 13 cm diameter), we found empirically that $b_{\mathrm{eff}} = 20$ cm. Although the ratio $b_{\mathrm{eff}}/D = 0.55$ is in the range of what one would expect intuitively, it would be interesting to compare this empirical result against a first-principle theory prediction of b_{eff}/D. To the best of our knowledge, however, the two asymptotes of $S_\alpha(f)$ for spherical waves observed with a circular aperture have not yet been worked out in explicit form.

We used Clifford's model, Eq. (14), which predicts an $f^{-8/3}$ asymptote for $f > f_k$, and we expect that a high-frequency asymptote with a dropoff steeper than $f^{-8/3}$ (such as $f^{-11/3}$, as predicted by Hogge and Butts [10] for a spherical wave observed with a circular, filled aperture) would provide only slightly different results. In other words, we expect the method to be quite robust with respect to changes in the actual high-frequency power law, as long as $S_\alpha(f)$ drops steeply at high frequencies.

Unfortunately, the described retrieval technique is insensitive to the sign of the cross-path wind. That is, it is difficult to separate a zero-mean, transverse wind speed that fluctuates during the observation period and/or along the propagation path with an rms value of σ_v from a constant transverse wind speed v_b comparable with σ_v. Future work could take advantage of spatial filtering [25,26] with the goal of manipulating the path-weighting function in order to obtain range-resolved wind retrievals, as opposed to path averages. This could include analyzing frequency cross spectra of AOAs from pairs of point sources observed simultaneously, either with the same aperture or with spaced apertures.

ACKNOWLEDGMENTS

We thank Dan Wolfe and Chris Fairall for helpful discussions and providing access to the BAO site. Thanks are

also owed to Steve Clifford, Rod Frehlich, Reg Hill, Rich Lataitis, and Doug Looze for their interest and encouragement, and to two reviewers for their valuable comments. A. Muschinski is the first holder of the Jerome M. Paros Endowed Professorship in Measurement Sciences at the University of Massachusetts at Amherst, and he thanks Linda and Jerome Paros for their generous support. This material is based on work supported in part by the U.S. Army Research Laboratory and the U.S. Army Research Office under grant 49393-EV and by the National Science Foundation under grant ATM-0444688.

REFERENCES

1. G. I. Taylor, "The spectrum of turbulence," Proc. R. Soc. London, Ser. A **164**, 476–490 (1938).
2. V. I. Tatarskii, *Wave Propagation in a Turbulent Medium* (McGraw-Hill, 1961).
3. V. I. Tatarskii, *The Effects of the Turbulent Atmosphere on Wave Propagation* (Israel Program for Scientific Translation, 1971).
4. A. S. Gurvich, M. A. Kallistratova, and N. S. Time, "Fluctuations in the parameters of a light wave from a laser during propagation in the atmosphere," Radiophys. Quantum Electron. **11**, 1360–1370 (1968).
5. S. F. Clifford, "Temporal-frequency spectra for a spherical wave propagating through atmospheric turbulence," J. Opt. Soc. Am. **61**, 1285–1292 (1971).
6. R. Rao, S. Wang, X. Liu, and Z. Gong, "Turbulence spectrum effect on wave temporal-frequency spectra for light propagating through the atmosphere," J. Opt. Soc. Am. A **16**, 2755–2761 (1999).
7. A. Lüdi and A. Magun, "Near-horizontal line-of-sight millimeter-wave propagation measurements for the determination of outer length scales and anisotropy of turbulent refractive index fluctuations in the lower troposphere," Radio Sci. **37**, 12.1–12.19 (2002).
8. R. S. Lawrence and J. W. Strohbehn, "A survey of clear-air propagation effects relevant to optical communications," Proc. IEEE **58**, 1523–1545 (1970).
9. Y. Cheon and A. Muschinski, "Closed-form approximations for the angle-of-arrival variance of plane and spherical waves propagating through homogeneous and isotropic turbulence," J. Opt. Soc. Am. A **24**, 415–422 (2007).
10. C. B. Hogge and R. R. Butts, "Frequency spectra for the geometrical representation of wavefront distortions due to atmospheric turbulence," IEEE Trans. Antennas Propag. **AP-24**, 144–154 (1976).
11. G. A. Tyler, "Bandwidth considerations for tracking through turbulence," J. Opt. Soc. Am. A **11**, 358–367 (1994).
12. D. S. Acton, R. J. Sharbaugh, J. R. Roehrig, and D. Tiszauer, "Wave-front tilt power spectral density from the image motion of solar pores," Appl. Opt. **31**, 4280–4284 (1992).
13. D. R. McGaughey and G. J. M. Aitken, "Temporal analysis of stellar wave-front-tilt data," J. Opt. Soc. Am. A **14**, 1967–1974 (1997).
14. F. F. Hall, "The Boulder Atmospheric Observatory," Opt. News **3** (2) 14–18 (1977).
15. J. C. Kaimal and J. E. Gaynor, "The Boulder Atmospheric Observatory," J. Clim. Appl. Meteorol. **22**, 863–880 (1983).
16. Lord Rayleigh, "Investigations in optics, with special reference to the spectroscope," Philos. Mag. **VIII**, 261–274 (1879).
17. A. S. Gurvich and M. A. Kallistratova, "Experimental study of the fluctuations in angle of incidence of a light beam under conditions of strong intensity fluctuations," Radiophys. Quantum Electron. **11**, 37–40 (1968).
18. R. Berry and J. Burnell, *The Handbook of Astronomical Image Processing* (Willmann-Bell, 2005).
19. S. B. Howell, *Handbook of CCD Astronomy* (Cambridge U. Press, 2000).
20. N. S. Nightingale and D. F. Buscher, "Interferometric seeing measurements at the La Palma Observatory," Mon. Not. R. Astron. Soc. **251**, 155–166 (1991).
21. M. A. Kallistratova and A. I. Kon, "Fluctuations in the angle of arrival of light waves from an extended source in a turbulent atmosphere," Izv. Vyssh. Uchebn. Zaved., Radiofiz. **9**, 636–639 (1966).
22. H. A. Panofsky and J. A. Dutton, *Atmospheric Turbulence Models and Methods for Engineering Applications* (Wiley, 1984).
23. R. W. Lee and J. C. Harp, "Weak scattering in random media, with applications to remote probing," Proc. IEEE **57**, 375–406 (1969).
24. A. D. Wheelon, *Electromagnetic Scintillation. I. Geometrical Optics* (Cambridge U. Press, 2001).
25. R. W. Lee, "Remote probing using spatially filtered apertures," J. Opt. Soc. Am. **64**, 1295–1303 (1974).
26. S. F. Clifford and R. J. Lataitis, "Spatial and temporal filtering of scintillation in remote sensing," IEEE Trans. Antennas Propag. **AP-35**, 597–604 (1987).